Neurotoxicology 93 (2022) 311–323

Contents lists available at ScienceDirect

Neurotoxicology

journal homepage: www.elsevier.com/locate/neuro

Acute, sub-chronic and chronic exposures to TiO_2 and Ag nanoparticles differentially affects neuronal function *in vitro*

Lora-Sophie Gerber [a,b,1], Harm J. Heusinkveld [a,b,1], Celine Langendoen [a], Burkhard Stahlmecke [c], Roel PF Schins [d], Remco HS Westerink [a,*]

[a] Institute for Risk Assessment Sciences (IRAS), Faculty of Veterinary Medicine, Utrecht University, Utrecht, the Netherlands
[b] National Institute for Public Health and the Environment (RIVM), P.O. Box 1, 3720 Bilthoven, BA, the Netherlands
[c] Institute of Energy and Environmental Technology e. V. (IUTA), Duisburg, Germany
[d] IUF - Leibniz Research Institute for Environmental Medicine, Duesseldorf, Germany

ARTICLE INFO

Edited by Yukun Yuan

Keywords:
Engineered nanomaterials
In vitro neurotoxicity testing
Silver nanoparticles
Titanium dioxide nanoparticles
Microelectrode array
Calcium imaging

ABSTRACT

In vivo toxicokinetic studies provide evidence for the translocation and accumulation of nanoparticles (NP) in the brain, thereby causing concern for adverse health effects, particularly for effects following chronic exposure. To date, only few studies investigated the effects of NP exposure on neuronal function in vitro, primarily focusing on short-term effects. The aim of this study was therefore to investigate the effects of two common types of NP, titanium dioxide NP (TiO_2NP) and silver NP (AgNP), on neuronal function following acute (0.5 h), sub-chronic (24 h and 48 h) and chronic (14 days) exposure in vitro. Effects of NP exposure on intracellular calcium homeostasis, spontaneous neuronal (network) activity and neuronal network morphology were investigated in rat primary cortical cells using respectively, single-cell microscopy calcium imaging, micro-electrode array (MEA) recordings and immunohistochemistry. Our data demonstrate that high doses of AgNP ($\geq$ 30 μg/mL) decrease calcium influx after 24 h exposure, although neuronal activity is not affected following acute and sub-chronic exposure. However, chronic exposure to non-cytotoxic doses of AgNP (1–10 μg/mL) potently decreases spontaneous neuronal (network) activity, without affecting network morphology and viability. Exposure to higher doses ($\geq$ 30 μg/mL) affects network morphology and is also associated with cytotoxicity. In contrast, acute and sub-chronic exposure to TiO_2NP is without effects, whereas chronic exposure only modestly reduces neuronal function without affecting morphology. Our combined findings indicate that TiO_2NP exposure is of limited hazard for neuronal function whereas AgNP, in particularly during chronic exposure, has profound effects on neuronal (network) function and morphology.

1. Introduction

Due to their very small size range (1–100 nm), engineered nanoparticles (NP) are used as additives in many applications (Oberdörster et al., 2009; Teleanu et al., 2018). The unique physicochemical properties and reactivity of NP are determined by size, but also by their shape, surface characteristics, and inner structure (for details see Shi et al., 2013). With decreasing diameter, the surface area of NP increases exponentially in relation to its mass and volume (Oberdörster et al., 2005), thereby potentially facilitating interaction with biological structures (Shi et al., 2013; Trouiller et al., 2009).

Titanium dioxide NP (TiO_2NP) and silver NP (AgNP) are among the most widely used NP. TiO_2NP have been commonly used in consumer products, such as cosmetics, toothpaste, sunscreen, paints, and pharmaceutical preparations (Shukla et al., 2011; Weir et al., 2012; Inshakova and Inshakov, 2017), whereas AgNP are well-known for their strong antimicrobial properties and use in coatings, textiles, wound dressings, biomedical devices, and personal care products (Strużyńska and Skalska, 2018). For most NP, inhalation and ingestion are the most relevant exposure routes. When inhaled, a large fraction of NP deposits in the nasal cavity, where they can enter brain structures directly via the dendrites of olfactory neurons that extend into the nasal cavity

* Correspondence to: Neurotoxicology Research Group, Division of Toxicology, Institute for Risk Assessment Sciences (IRAS), Faculty of Veterinary Medicine, Utrecht University, P.O. Box 80.177, NL-3508 TD Utrecht, the Netherlands.
E-mail address: R.Westerink@uu.nl (R.H. Westerink).
[1] Both authors contributed equally to this study.

https://doi.org/10.1016/j.neuro.2022.10.010
Received 19 July 2022; Received in revised form 7 October 2022; Accepted 17 October 2022
Available online 22 October 2022

(Oberdörster et al., 2004; Wang et al., 2008b, 2008a; Boyes and van Thriel, 2020). Additionally, NP can also translocate through biological barriers, such as lung epithelium and intestinal mucosa, to reach the systemic circulation (Geraets et al., 2014; Kreyling et al., 2017). Both in vivo and in vitro studies indicated that NP can cross the blood-brain-barrier (Guo et al., 2020; Li et al., 2010; Skalska et al., 2016; Tang et al., 2010, 2009) and several studies detected elemental Ti and Ag in the brains of exposed animals suggesting that NP can enter brain structures (Gao et al., 2011; Grissa et al., 2020; Hu et al., 2010; Hu et al., 2011; Lee et al., 2013; Skalska et al., 2015; Sofranko et al., 2021; Tang et al., 2010, 2009; Wang et al., 2008b; Ze et al., 2014; Boyes and van Thriel, 2020). Notably, Ag remained present in brains post-exposure, indicating a slow elimination rate that can lead to accumulation in several brain structures (Lee et al., 2013; Sofranko et al., 2021; van der Zande et al., 2012).

Metal-based engineered NP have been reported to induce in vivo neurotoxicity, including changes in sensory, motor and cognitive function such as learning and memory, as well as changes in autonomic functions, brain morphology, and brain biochemistry (Bencsik et al., 2018; Sharma and Sharma, 2012; Sharma et al., 2009; Yokel et al., 2013; Yokel and Macphail, 2011; Teleanu et al., 2019; Boyes and van Thriel, 2020). Furthermore, both in vitro and in vivo studies demonstrated that AgNP exposure inhibits neurite outgrowth, causes ultrastructural changes in synapses including disruption of synaptic membranes, leads to degeneration of synapses and neurites, and is associated with increased presence of myelin-like structures that are linked to neurodegenerative processes (Repar et al., 2018; Skalska et al., 2015; Xu et al., 2013). It has been suggested that many of the neurotoxic effects of NP are related to general toxic mechanisms (e.g., oxidative stress and eventually cell death) as well as neuron- or glia cell-specific mechanisms (e.g., synaptic degeneration and neuroinflammation) causing perturbations of neurotransmission and neuroplasticity, and subsequent neurodegeneration (for review see Boyes and van Thriel, 2020).

Only a few studies investigated the effect of NP exposure on neuronal function in vitro and revealed that several NP affect neuronal activity and network pattern in the absence of general cytotoxicity (Gramowski et al., 2010; Strickland et al., 2016, 2015). Strickland et al., (2015, 2016) screened several metal oxide NP, including TiO_2NP and AgNP, for their potency to change neuronal activity. In those studies, it was shown that changes in neuronal network activity occurred mostly after 48 h exposure and following external stimulation, but also that for some NP a transient impairment of the activity was seen upon short-term exposure for 1 h. Those studies only monitored neuronal (network) activity for up to 48 h. However, the evidence of NP accumulation in the brain, the limited repair capacity of neuronal structures, and the slow onset of neurodegenerative diseases (Boyes and van Thriel, 2020) highlight the need for chronic exposure experiments in order to further characterize the hazard of NP.

We therefore assessed the impact of TiO_2NP and AgNP on neuronal (network) activity in rat primary cortical cultures following acute (0.5 h), sub-chronic (24 h and 48 h) and 14 days chronic exposure. While these primary cultures no longer have a direct relation to in vivo neuroanatomy, rat primary cortical cultures are the current gold standard in in vitro neurotoxicity testing and contain a multitude of cellular targets that are essential for neuronal function. When cultured on microelectrodes arrays (MEA), primary cortical cultures develop spontaneous neuronal network activity within a couple of days in vitro (DIV). Neuronal network activity is characterized by synchronized network bursting which resembles the in vivo situation (Charlesworth et al., 2015), and can be used as an efficient approach for neurotoxicity screening (for review see Gerber et al., 2021). We could thus monitor effects of NP exposure on neuronal network function in a non-invasive manner in parallel cultures exposed for up to 14 days. Further, we investigated the effects of sub-chronic (24 h) exposure to TiO_2NP and AgNP on calcium (Ca^{2+}) homeostasis, in particularly Ca^{2+} influx through voltage-gated calcium channels (VGCCs), which are critical for neurotransmission (Westerink, 2006) and are involved in neurodegeneration (Mattson, 2007). Additionally, exposed cultures were stained at several time points to determine effects on neuronal network and astrocytes morphology to gain additional insight in the effects of chronic exposure to TiO_2NP and AgNP on neuronal networks.

2. Materials and methods

2.1. Chemicals

Fetal bovine serum (FBS), Neurobasal-A (NBA) medium, L-glutamine, penicillin-streptomycin (10.000 U/mL–10.000 µg/mL), Hanks' Balanced Salt Solution (HBSS), Phosphate-buffered saline (PBS), 4′,6-diamidino-2-phenylindole (DAPI), and goat anti-rabbit Alexa Fluor® 568 were obtained from Life Technologies (Bleiswijk, The Netherlands). Fura-2-AM (Fura-2-acetoxymethyl ester) was purchased from Molecular Probes (Invitrogen, Breda, The Netherlands). Paraformaldehyde (PFA) was obtained from Electron Microscopy Sciences (Hatfield, Pennsylvania, USA). Rabbit anti-β(III)-tubulin (Ab18207) and mouse anti-S100β (Ab11178) were obtained from Abcam (Cambridge, United Kingdom). Donkey anti-mouse Alexa Fluor® 488 was obtained from Jackson ImmunoResearch (Ely, United Kingdom). ProLong™ Diamond Antifade Mountant was purchased from Thermo Fisher Scientific (Breda, The Netherlands). Unless otherwise indicated, all other chemicals were obtained from Sigma Aldrich (Zwijndrecht, The Netherlands). Saline solutions for intracellular calcium imaging, containing (in mM) 125 NaCl, 5.5 KCl, 2 $CaCl_2$, 0.8 $MgCl_2$, 10 HEPES, 24 glucose and 36.5 sucrose (pH 7.3, adjusted using HCl), were prepared with de-ionized water (Milli-Q®; resistivity >18 MΩ·cm).

2.2. Nanomaterial

TiO_2NP was obtained from the Joint Research Center of the EU (JRC) (NM105; fumed TiO_2 obtained by flame pyrolysis of Titanium tetrachloride, originally from Evonik Degussa GmbH), with an average primary particle size of 26.2 ± 10.7 nm. AgNP was obtained from Sigma Aldrich (#576832; 0.2 % polyvinylpyrrolidone (PVP)-coated) with an average primary particle size of 40.2 ± 17.6 nm. Just prior to exposure, NP stock suspensions (2.56 mg/mL) were freshly prepared in Milli-Q® + 2 % FBS using ultrasonic bath (Bandelin SONOREX, BANDELIN electronic GmbH, Germany) for 15 min, and further diluted in FBS medium (450 mL NBA medium supplemented with 14 g sucrose, 1.25 mL L-glutamine (200 mM), 5 mL Penicillin/streptomycin and 50 mL FBS, pH 7.4) to obtain NP working suspensions (1 mg/mL).

2.3. Nanomaterial characterization

When suspended, particles are usually present as agglomerates of different sizes. Therefore, we assessed the suspension states of the TiO_2NP and AgNP suspension, size distribution, and the size and morphology of agglomerates by scanning electron microscopy (SEM) analysis and dynamic light scattering (DLS) analysis. To characterize NP under the applied cell culture testing conditions, NP working suspensions (1 mg/mL) were prepared as described above (see section Nanomaterial).

To evaluate the morphology, the size distribution (mean and mode diameter), and aspect ratio (width/length) of suspended TiO_2NP and AgNP, dried NP suspensions were visualized using scanning electron microscopy as described previously (Kämpfer et al., 2021; Sofranko et al., 2021). To do so, 10 µL of the NP suspensions were pipetted on 0.2 µm pore size Whatman filters. Air-dried filters were coated with a 10 nm gold layer and subsequently analyzed using a field emission scanning electron microscope (7500 F, JEOL (Germany) GmbH, Germany). Images were captured at magnifications between 50x and 50.000x for an overview of the sample distribution and at 10.000x or 25.000x to perform size analysis of NP. Per sample, 300 agglomerates were

analyzed using ImageJ (version 1.51 f, see http://imagej.nih.gov/ij). Since agglomerates were asymmetrical, the diameter of each of the 300 agglomerates was measured twice to obtain the maximum and minimum Feret diameters and the resulting 600 values were used to determine the mean diameters, mode diameters and aspect ratios.

To evaluate the stability of the NP suspensions, DLS measurements were performed directly (0 h), 0.5 h, 6 h, 24 h, and 48 h after preparation of NP stock suspension. Until analysis, TiO_2NP and AgNP stock suspensions were kept at humidified 5 % CO_2/95 % air atmosphere at 37 °C. For DLS measurement, samples from the top of the NP stock suspension (in triplicates) were taken at the indicated time points and analyzed using a Delsa Nano C particle analyzer (Beckman Coulter GmbH, Krefeld, Germany). Samples were not vortexed or sonicated before each measurement, but only during preparation of the NP stock suspension. Hydrodynamic diameter (z-average) and polydispersity index (PDI) of the NP suspensions were determined based on the obtained intensity.

2.4. In vitro dosimetry using ISDD

The applied dose, presented in NP concentrations (μg/mL), does not provide accurate information about the actually available dose (delivered dose), which depends on the deposition of NP and agglomerates (Cohen et al., 2014). Therefore, the In vitro Sedimentation, Diffusion and Dosimetry (ISDD) model (Hinderliter et al., 2010) was used to simulate the delivered dose for acute and sub-chronic exposure to NP as a function of time. Simulations were performed using the ISDD graphic user interface with MATLAB Compiler Runtime v8.3 R2014a. The required input parameters were determined as follows: primary particle sizes and specific material density were given by the manufacturer. Agglomerate diameters were obtained by scanning electron microscopy. For the stacking factor, the theoretical value of 0.634 (for random stacking of uniform spheres) was applied (DeLoid et al., 2014). Effective densities of particle agglomerates were estimated by volumetric centrifugation according to Deloid et al. (2014). Briefly, particle suspensions of 100 μg/mL in FBS medium (dispersed as described above) were centrifuged for 1 h at 3000xg in packed cell volumes tubes. Subsequently, the volume that is occupied by the particle agglomerates was measured and used to determine the effective density. Values for refractive index, density, and viscosity of the FBS medium were taken from literature (see Strickland et al., 2015). Sedimentation simulations were run for acute (0.5 h exposure), sub-chronic (24 h and 48 h exposure) and chronic MEA experiments until the first medium change on DIV10 after 3 days (72 h) of exposure. In case of TiO_2NP, simulation was performed for 30 μg/mL for acute and sub-chronic exposure experiment and for 30 μg/mL and 100 μg/mL for chronic exposure experiment. For AgNP, the highest concentration was 100 μg/mL for both setups, which is why sedimentation was only simulated for this concentration. Simulation results are presented as deposited mass in μg and deposited fraction in % of applied dose.

2.5. Cell culture

Animal experiments were performed in agreement with Dutch law, the European Community directives regulating animal research (2010/63/EU), and approved by the Ethical Committee for Animal Experiments of Utrecht University. All efforts were made to minimize the number of animals used and their suffering.

Rat primary cortical cultures form a dense network of neurons and astrocytes (see Supplementary data Fig. S1). Rat primary cortical cells were isolated from the cortex of Wistar rat pups at postnatal day 0–1 as described previously (Gerber et al., 2021; Nicolas et al., 2014) with minor modifications. Briefly, rat pups were decapitated and the cortex was isolated and placed in dissection medium (450 mL NBA medium, supplemented with 14 g sucrose, 1.25 mL L-glutamine (200 mM), 5 mL glutamate (3.5 mM), 5 mL penicillin/streptomycin, 50 mL FBS and pH adjusted to 7.4). Cortices were minced and triturated to a homogenous suspension and filtered through an easy strainer (100 μm, Greiner Bio One, Alphen aan den Rijn, The Netherlands). Subsequently, cells were centrifuged for 5 min at 100xg. The supernatant was removed and the pellet was resuspended in dissection medium. To culture rat primary cortical cells on plastic, glass, and microelectrode arrays (mwMEA, Axion BioSystems Inc, Atlanta, USA, M768-GL1–30Pt200), all culture surfaces were coated with 0.1 % polyethyleneimine (in borate buffer (24 mM sodium borate/50 mM boric acid; pH 8.4)) prior to cell isolation (Gerber et al., 2021).

For cell viability experiments, rat primary cortical cells were seeded at a density of 1×10^5 cells/well in 500 μL on 48-well plates. For single-cell intracellular calcium (Ca^{2+}) imaging experiments, 4×10^5 cells were seeded per dish in a 200 μL on the glass of glass-bottom dishes (MatTek, Ashland, MA, USA). The cells were allowed to adhere to the glass for 2 h after which 200 μL dissection medium was added. For MEA experiments and immunohistochemistry, cells were seeded at 1×10^5 cells/well in a 50 μL droplet directly on the electrode array of a 48-well MEA plate (Axion Biosystems Inc., Atlanta, GA, USA) and glass bottom of 8-well micro-slides (Ibidi, Gräfelfing, Germany), respectively. Similar to cells seeded on glass-bottom dishes for Ca^{2+} imaging experiments, cells were allowed to adhere to the electrode array or glass-bottom for 2 h after which 450 μL or 250 μL dissection medium was added to each well of the 48-well MEA plate or 8-well micro-slides, respectively.

Rat primary cortical cells were maintained in a humidified 5 % CO_2/95 % air atmosphere at 37 °C. On the day following seeding (one day in vitro (DIV1)), dissection medium was replaced by glutamate medium (500 mL NBA medium supplemented with 14 g sucrose, 1.25 mL L-glutamine (200 mM), 5 mL glutamate (3.5 mM), 5 mL penicillin/streptomycin and 10 mL B-27, pH 7.4). For cells grown on MEA plates, only 450 μL dissection medium was replaced by 450 μL glutamate medium to avoid mechanical damage of the electrodes by pipet tips. On DIV4, glutamate medium was replaced by FBS medium. For cell viability, chronic exposure MEA experiments, and immunohistochemistry, primary cells were maintained by refreshing 50 % of the FBS medium every 3–4 days.

2.6. Intracellular calcium imaging

The effect of TiO_2NP and AgNP on basal intracellular Ca^{2+} level ($[Ca^{2+}]_i$) and depolarization-evoked Ca^{2+}-influx was investigated on a single cell level using the Ca^{2+}-sensitive fluorescent ratio dye Fura-2 AM as described previously (Heusinkveld et al., 2016). Experiments were performed on DIV9–11, which relates to the time frame during which the cortical cells show highly synchronized spontaneous neuronal activity (Dingemans et al., 2016).

Rat primary cortical cells were exposed to 1–30 μg/mL TiO_2NP and AgNP 24 h prior to Ca^{2+} imaging experiments. Due to technical limitations (overload of the glass bottom dish with NP), exposure to 100 μg/mL was not included in these experiments. After 24 h exposure, cells were loaded by incubation with 5 μM Fura-2 AM (in saline solution) for 20 min at room temperature (RT), followed by washing with saline solution and resting for 15 min to allow de-esterification of Fura-2 AM. After de-esterification, the cells were placed on the stage of an Observer A1 inverted microscope (Zeiss, Göttingen, Germany) equipped with a Lambda DG-4 illumination system (Sutter Instrument Company, Novato CA, USA). After a 5 min baseline recording, cells were depolarized by high-K^+ containing saline (KCl increased to 100 mM, NaCl reduced to 25 mM) for 27 s to investigate effects of TiO_2NP and AgNP on the depolarization-evoked increase in $[Ca^{2+}]_i$. High-K^+ containing saline provides a robust depolarization to ~0 mV, which is sufficient to open both high- and low voltage-activated voltage-gated calcium channels (VGCCs). Fluorescence, evoked by 340 and 380 nm excitation wavelengths (F340 and F380), was recorded every 3 s at 510 nm with a CoolSNAP™ MYO CCD camera (Photometrics, Tucson, AZ, USA). Changes in the F340/F380 ratio, reflecting changes in $[Ca^{2+}]_i$, were

further analyzed using custom-made MS-Excel macros calculating F340/F380 ratios and applying a correction for background fluorescence (Heusinkveld et al., 2016).

The amplitude of $[Ca^{2+}]_i$ within a minute of the start of depolarization was determined per cell, and the net increase (amplitude $[Ca^{2+}]_i$ – basal $[Ca^{2+}]_i$ during the last minute prior to depolarization) was used to investigate effects of NP on depolarization-evoked $[Ca^{2+}]_i$. The results represent the depolarization-evoked net increase in $[Ca^{2+}]_i$ in treated cells as percentage of the depolarization-evoked net increase in $[Ca^{2+}]_i$ in control cells.

2.7. MEA experiments

MEA recordings were used to investigate acute (0.5 h), sub-chronic (24 h and 48 h), and chronic (14 days) effects following a single exposure to TiO_2NP and AgNP on spontaneous neuronal activity and network connectivity (for a detailed description of the experimental procedure for MEA recordings also see Gerber et al., 2021). Each MEA recordings comprised of 5 min acclimatization period followed by 30 min recording of the neuronal (network) activity at 37 °C. Axion's Integrated Studio (AxIS 1.7.8) was used for data acquisition of spontaneous neuronal activity during acute, sub-chronic and chronic MEA experiments. Channels were sampled at 12.5 kHz, signals were pre-amplified with a gain of 1200 × (61 dB), and band-pass filtered at 0.2–5 kHz. A cell-free MEA experiment was performed to test if AgNP affect the noise levels of the electrodes since Ag is a highly conductive metal. A 48-well MEA plate containing only FBS medium was recorded for 10 min and exposed afterwards to FBS medium (control) or 100 μg/mL AgNP. After 14 days exposure another 10 min MEA recording took place. Average noise level of electrodes assessed before and after exposure to FBS medium and 100 μg/mL AgNP did not differ from level before exposure or wells exposed to FBS medium (Supplementary data Fig. S2) indicating that MEA recording were not affected by AgNP.

2.7.1. Acute and sub-chronic exposure MEA experiments

For acute and sub-chronic exposure experiments, baseline neuronal activity of rat primary cortical cells was recorded on DIV9. Subsequently, cells were exposed once to TiO_2NP or AgNP (1–100 μg/mL) under sterile conditions and neuronal activity was recorded immediately afterwards (acute MEA recording). Next, cells were maintained in a humidified 5 % CO_2/95 % air atmosphere at 37 °C and further MEA recordings were performed on DIV10 and DIV11, i.e., after 24 h and 48 h exposure, respectively.

2.7.2. Chronic exposure MEA experiments

On DIV7, a baseline MEA recording was performed and cells were subsequently exposed to 1–100 μg/mL TiO_2NP and AgNP by replacing 50 % of the medium with glutamate-free culture medium containing NP. Afterward, cells were maintained in a humidified 5 % CO_2/95 % air atmosphere at 37 °C. Further MEA recordings took place on DIV10, DIV14, DIV17, and DIV21 and a half-medium change was performed following each MEA recording.

2.8. Cell viability assay

Rat primary cortical cells were exposed for 14 days to 1–100 μg/mL TiO_2NP or AgNP, starting on DIV7. Cells were maintained until DIV21 by refreshing 50 % of the FBS medium every 3–4 days. After 14 days of exposure (DIV21), an Alamar Blue assay was performed (protocol adapted from Bopp and Lettieri, 2008) to measure mitochondrial activity as a readout of cell viability. Briefly, exposure medium was replaced by 300 μL 25 μM Alamar Blue solution in HBSS (Invitrogen, Breda, The Netherlands) and cells were incubated for 75 min at 37 °C. For fluorescence measurement of resorufin, 200 μL of the Alamar Blue solution was then transferred from each well to a transparent 96-well (Gerber et al., 2021). Conversion of resazurin to resorufin was measured spectrophotometrically at 540/590 nm (Infinite M200 microplate; Tecan Trading AG, Männedorf, Switzerland).

2.9. Immunohistochemistry

Cells were exposed to 30 μg/mL TiO_2NP or 3 μg/mL and 30 μg/mL AgNP on DIV7. Due to an overload of NP when exposing to 100 μg/mL (resulting in high background level during imaging), this dose was not included in the immunohistochemistry experiment. On DIV10, DIV14 and DIV21, rat primary cortical cells were fixated and immunofluorescent stained with antibodies specific for neurons (anti-β(III) tubulin) and astrocytes (anti-S100β) accompanied by nuclear staining (DAPI) as described previously (Tukker et al., 2016). Briefly, micro-slides were first fixated with 4 % PFA in 0.1 M PBS (pH 7.4) at room temperature (RT) for 20 min followed by 20 min quenching for PFA, permeabilization and blocking by incubating with 20 mM NH_4Cl in blocking buffer (2 % bovine serum albumin and 0.1 % saponin in PBS) at RT. Next, the micro-slides were incubated overnight at 4 °C in blocking buffer with rabbit anti-β(III) tubulin (final dilution 1:250) and mouse anti-S100β (final dilution 1:500). Each of the subsequent wash and incubation steps was performed in blocking buffer. Micro-slides were washed 3 times and incubated with donkey anti-mouse Alexa 488 and goat anti-rabbit Alexa 568 at a final dilution of 1:100 for 1 h at RT in the dark. Subsequently, nuclear staining was performed by incubating the coverslips with DAPI at a concentration of 300 nM for 2–3 min at RT in the dark. Washing procedure was repeated and coverslips were sealed with ProLong™ Diamond Antifade Mountant. Immunofluorescent stained micro-slides were visualized with an Olympus BX60 fluorescence microscope (equipped with Leica DFC425C color CCD camera (5 Megapixels) using a 20x UPlanfluor objective (N.A. 0.5). Images were captured as 16 bit.tiff files using Leica Application Suite (LAS AF version 4.7; Leica Microsystems GmbH, Wetzlar, Germany).

2.10. Data analysis and statistics

Data from single-cell fluorescence microscopy reflecting depolarization-evoked changes in net $[Ca^{2+}]_i$ increase are presented as F340/F380 ratio (R) normalized to control ratio. The data represent average values ± standard error of the mean (SEM; calculated using *n*) derived from 58 to 90 individual cells (*n*) in 4 independent experiments (*N*). Analysis via one-way ANOVA followed by a post-hoc Dunnet's test was used to compare depolarization-evoked net increase in $[Ca^{2+}]_i$ in cells following NP exposure compared to control cells.

Acute and sub-chronic MEA data were generated in 3 independent experiments (*N*) with at least 3 biological replicates per experiment ($n \geq 9$). Chronic exposure MEA data set consist of 3–4 independent experiments (*N*) with at least 3 biological replicates per experiment ($n = 13–23$). To determine effects of NP on neuronal (network) activity, spike, burst, network burst parameter are presented as % mean ± SEM (calculated using *n*) compared to time-matched control.

MEA data processing and analysis was performed as described previously (Gerber et al., 2021). Briefly, raw data was re-recorded and spikes were detected using the AxIS spike detector (Adaptive threshold crossing, Ada BandFlt v2) with a post/pre spike duration of 3.6/2.4 ms and a spike threshold of 7 × SD of the internal noise level (rms) of each individual electrode. Next, average values of spikes (mean spike rate, MSR), bursts (mean burst rate, MBR), and network bursts (mean network burst rate, MNBR) were determined using NeuroExplorer 5.007 software (Nex Technologies, Madison, WI, USA). Only wells containing > 4 active electrodes (≥ 6 spike/min) in the baseline recording were included. Bursts were defined using the Poisson surprise method (minimum of 10 surprises). Network bursts were defined using

inter-spike-interval threshold with a minimum of 40 spikes, each separated by a maximum of 100 ms, for a minimum of 15 % of the electrodes/well.

For acute and sub-chronic experiments, the last 10 min of baseline and exposure recording were used for analysis since this was the most stable timeframe (see Hondebrink et al., 2016 for details). For each well, a treatment ratio per parameter and time point (0.5 h, 24 h, and 48 h) was calculated as followed:

$$Treatment\ ratio_{\ acute\ /\ sub-chronic} = \frac{MEA\ parameter\ value_{\ exposure\ recording}}{MEA\ parameter\ value_{\ baseline\ recording}}$$

Next, outlier analysis (mean ± 2x SD) of control wells (0 % outliers) per independent experiment was performed first and MEA parameters of NP exposed wells were normalized to mean control values. Finally, results of independent experiments were combined and outlier analysis was performed for NP exposed wells (mean ± 2x SD; 4.7 % outliers). Acute and sub-chronic MEA data are presented as % mean spike rate (MSR) and % mean network burst rate (MNBR) ± SEM (calculated using *n*) compared to time-matched control.

For chronic exposure experiments, treatment ratios were calculated for the last 20 min of chronic MEA recordings (DIV7, DIV10, DIV14, DIV17, DIV21). Per independent experiment, outliers (mean ± 2x SD) within control wells (3.9 % outliers) were excluded and raw values per time point of NP exposure wells were normalized to the mean value of their time-matched control by the following equation:

$$Treatment\ ratio_{chronic} = \frac{MEA\ parameter\ value_{\ exposure\ well\ (DIV\ 7-21)}}{MEA\ parameter\ value_{control\ well\ (DIV\ 7-21)}}$$

Results of independent experiments were combined and outlier analysis was performed for NP exposed wells (mean ± 2x SD; 4.9 % outliers). Finally, treatment ratios obtained for NP exposed wells for baseline recording on DIV7 were set to 100 % and treatment ratios for later DIVs were adapted accordingly to correct for potential differences in neuronal activity during baseline recording. Chronic MEA data are presented as % mean spike rate (MSR) and % mean network burst rate (MNBR) ± SEM (calculated using *n*) compared to time-matched controls.

Data from cell viability experiments were generated in 3 independent experiments ($N = 3$) consisting of at least 7 biological replicates per experiment ($n \geq 21$). Cell viability data are presented as % viability ± standard deviation (SD; calculated using *n*) compared to controls. Analysis via one-way ANOVA followed by a post-hoc Dunnet's test was used to determine significant effects of NP exposure on metabolic activity (as measure for cell viability) compared to control.

Statistical analyses were performed using GraphPad Prism v7 (GraphPad Software, San Diego, California, USA). A Welch's ANOVA followed by a Dunnett's T3 multiple comparisons test (for acute and sub-chronic MEA data) or a two-way ANOVA followed by a Dunnett's T3 multiple comparisons test (chronic MEA data) was used to compare treatment ratios in NP exposed wells to treatment ratios in control wells.

3. Results

3.1. Nanomaterial characterization

Based on the scanning electron microscopy images, the morphology and number size distribution of suspended TiO_2NP and AgNP were assessed (Fig. 1, Table 1). Since the number size distribution is non-Gaussian, mean (average size) and mode diameter (frequency peak) are reported. Both nanomaterials tend to form bulky agglomerates in suspension with a mean diameter of 761.8 nm and 786.5 nm for TiO_2NP and AgNP, respectively, and an aspect ratio beyond 2 indicating an irregular shape of the agglomerates.

In suspension, the mode size of TiO_2 and Ag agglomerates is 200–400 nm. As indicated by the different values for the mean and the mode diameter and the size distribution histograms (Fig. 2), both NP suspensions exhibit a considerable quantity of bulky agglomerates with sizes exceeding 1000 nm. From Fig. 2 it also becomes apparent that size and shape characteristics of suspended TiO_2 and Ag are largely comparable.

To assess the stability of the NP suspensions in culture medium and over time, the hydrodynamic diameters (z-average) and polydispersity index (PDI) were determined by DLS analysis on several time points after NP suspensions were prepared (Fig. 3). Directly after suspension (0 h and 0.5 h), the hydrodynamic diameter of both suspended NP exceeds 1000 nm with a PDI above 0.4. After 6 h in suspension, the hydrodynamic diameter of TiO_2NP and AgNP decreases to 490 nm and 570 nm, respectively, and both suspensions exhibit a comparable PDI of 0.3. Subsequent DLS measurements at 24 h and 48 h after suspension show that the hydrodynamic size further decreases for both NP, indicating sedimentation of large bulky agglomerates. After 48 h, the hydrodynamic size for TiO_2NP and AgNP suspension amounts to 308 nm and 205 nm, respectively. However, the TiO_2NP suspension appears to

Table 1
Characteristics of TiO_2NP and AgNP suspensions assessed by SEM image analysis.

Nanomaterial	Mean diameter ± SD [nm]	Mode diameter ± SD [nm]	Mean aspect ratio ± SD
TiO_2NP	761.8 ± 795.2	223.4 ± 1.7	2.44 ± 0.77
AgNP	786.5 ± 879.7	232.6 ± 2.2	2.25 ± 0.68

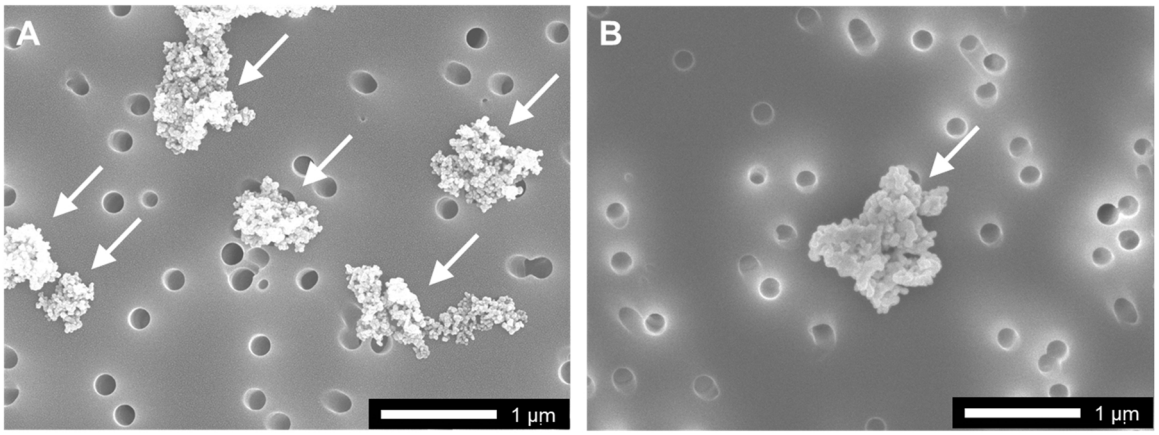

Fig. 1. Representative SEM images of (A) TiO_2 and (B) Ag agglomerates. NP suspension was applied on pore size Whatman filters, air-dried, and images were captured at 25.000x magnification. Particle agglomerates are marked with a white arrow. Filter pores can be seen as spheric objects on the images.

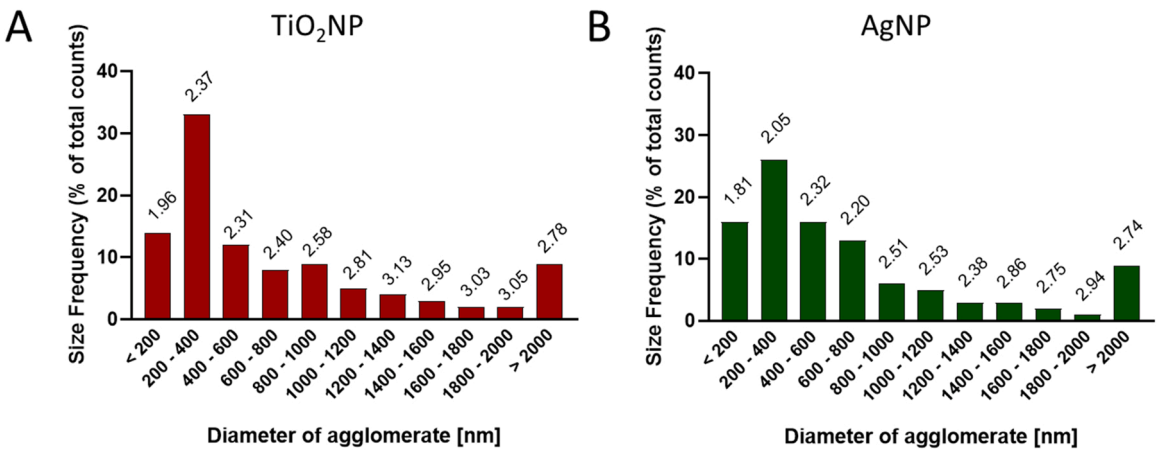

Fig. 2. Size distribution and aspect ratios of TiO_2 and Ag agglomerates in suspension assessed by scanning electron microscopy. Data are presented as the percentage of all counts (n = 300). Values above the bars indicate aspect ratios of the particular size range.

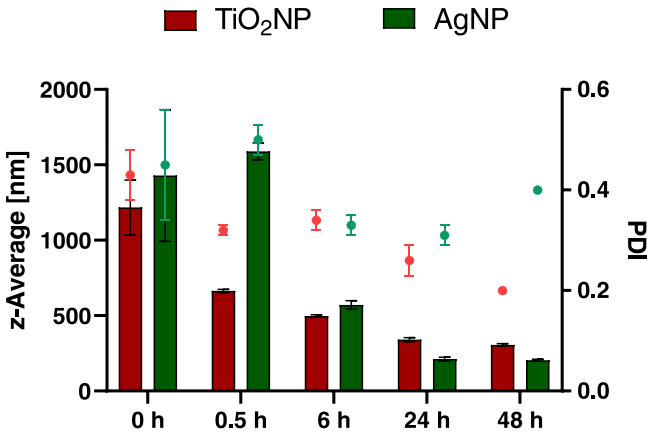

Fig. 3. Hydrodynamic diameter and polydispersity index (PDI) of TiO_2NP and AgNP suspended in FBS culture medium. Samples were analyzed by DLS. Bars represent z-average [nm] of TiO_2NP (red) and AgNP (green) assessed 0 h, 0.5 h, 6 h, 24 h, and 48 h after NP suspension and symbols depict corresponding PDI. Data show mean ± SD of 100 measurements, assessed in triplicates (n = 3).

be more stable since the PDI further decreases to 0.2, whereas 48 h after preparation the PDI of the AgNP suspension increases again to 0.4, which possibly indicates dissolution of AgNP.

3.2. Particle sedimentation modeling

For evaluation of the neurotoxic potency of TiO_2NP and AgNP, and to aid in vitro-in vivo extrapolation, it is important to relate the applied dose to the dose of NP delivered to the cells. The NP sedimentation rates differ due to different material, material density, size of primary particle and their agglomerates, and effective density of NP agglomerates, leading to varying delivered doses of the different NP samples (Cohen et al., 2014).

The estimated deposited fraction of TiO_2NP is ~4 times larger than for AgNP (Table 2). Comparing the deposited mass of both NP, the highest applied dose of TiO_2NP and AgNP, 30 μg/mL and 100 μg/mL respectively, lead to a comparable delivered dose in the acute and the sub-chronic MEA experiments (Table 2). Estimation for the chronic MEA experiments were done for 3 days exposure, when the first half-medium change took place. Here, the highest applied dose for both NP (100 μg/mL), results in a 4-fold higher delivered dose of TiO_2NP (36.2 μg/cm^2) compared to AgNP (9.4 μg/cm^2). Similar to the acute and sub-chronic exposures, an applied dose of 30 μg/mL TiO_2NP leads to a comparable deposited mass per surface area as estimated for 100 μg/mL applied AgNP.

Table 2
Deposited mass per surface area (μg/cm^2) and deposited fraction (%) of NP after several exposure durations during acute (0.5 h), sub-chronic (24 h and 48 h) and chronic (3 days) exposure experiments performed on MEA 48-well plates. Values were estimated using the ISDD model. Simulation was run with highest concentration used during the experiments.

	Acute and sub-chronic exposure experiments			
	TiO_2NP		AgNP	
Applied dose	30 μg/mL		100 μg/mL	
Delivered dose	Deposited mass per surface area	Deposited fraction	Deposited mass per surface area	Deposited fraction
0.5 h	0.14 μg/cm^2	0.7 %	0.33 μg/cm^2	0.5 %
24 h	3.8 μg/cm^2	19.2 %	3.8 μg/cm^2	5.8 %
48 h	7.5 μg/cm^2	38.0 %	6.7 μg/cm^2	10.3 %
	Chronic exposure experiments			
	TiO_2NP		AgNP	
Applied dose	30 μg/mL / 100 μg/mL		100 μg/mL	
Delivered dose	Deposited mass per surface area	Deposited fraction	Deposited mass per surface area	Deposited fraction
3 days	10.9 μg/cm^2 / 36.2 μg/cm^2	60.8 %	9.4 μg/cm^2	15.8 %

3.3. Intracellular calcium imaging

Proper neuronal signaling requires strict regulation of the intracellular calcium concentration $[Ca^{2+}]_i$, with a rapid but transient increase upon membrane depolarization (Barclay et al., 2005). We therefore investigated if 24 h exposure to TiO_2NP and AgNP affects basal $[Ca^{2+}]_i$ or depolarization-evoked net $[Ca^{2+}]_i$ increase using single-cell fluorescence microscopy in Fura-2-loaded rat primary cortical cultures.

Neither TiO_2NP (0.3–30 μg/mL) nor AgNP (0.3–30 μg/mL) affects basal $[Ca^{2+}]_i$ in rat primary cortical cells following 24 h of exposure (Supplementary data, Fig. S3). Also, no change in depolarization-evoked net $[Ca^{2+}]_i$ increase was observed for TiO_2NP up to 30 μg/mL (Fig. 4). However, 24 h exposure to AgNP induces a dose-dependent decrease of the depolarization-evoked net $[Ca^{2+}]_i$, with 68 % of control influx remaining for 30 μg/mL ($p < 0.001$), indicative for an inhibition of VGCC.

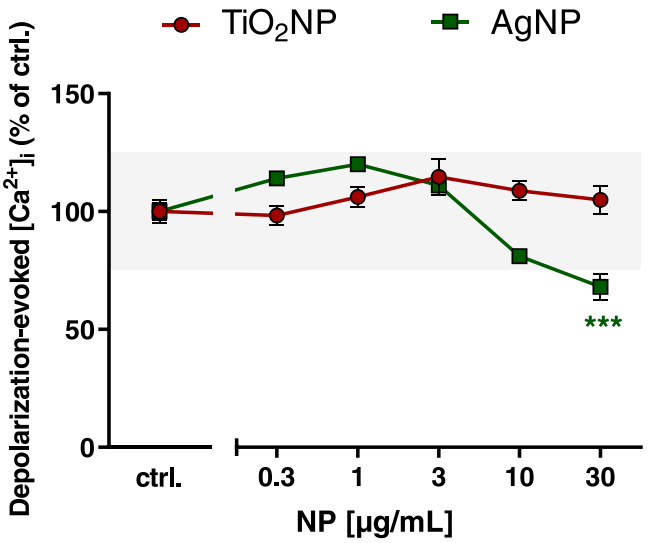

Fig. 4. Effect of 24 h exposure to TiO_2NP and AgNP on depolarization-evoked net increase in $[Ca^{2+}]_i$ in rat primary cortical cells measured using single cell fluorescence microscopy. Data are expressed as mean ± SEM of net $[Ca^{2+}]_i$ increase following depolarization (high K^+) as percentage of DMSO-exposed control cells, from n = 58–90 cells in N = 4 independent experiments. Effects ≤ 25 % (i.e. the variation of vehicle control) are considered to be of limited (toxicological) relevance (depicted by the grey area). Relevant effects that are statistically different (one-way ANOVA) from control are indicated with *** ($p < 0.001$).

3.4. MEA recordings after acute and sub-chronic exposure

To investigate if the effects on $[Ca^{2+}]$ homeostasis are also reflected in neuronal network function, we assessed if acute (0.5 h) and sub-chronic (24 h and 48 h) exposure to TiO_2NP and AgNP affects neuronal (network) activity in rat primary cortical cells by performing MEA recordings.

Acute (0.5 h) and 24 h sub-chronic exposure of rat primary cortical cells to TiO_2NP (3–30 µg/mL) does not affect MSR or MNBR (Fig. 5A). Following 48 h sub-chronic exposure to TiO_2NP, only a modest reduction in MSR (73–82 %) is observed, which is smaller than the relevant effect size and is therefore considered to be of limited toxicological relevance.

Acute (0.5 h) exposure to 100 µg/mL AgNP reduces MSR and MNBR to respectively 63 % ($p = 0.0038$) and 55 % ($p = 0.0152$) compared to time-matched controls (Fig. 5B). Although effects on MSR did not reach significance following 24 h exposure, MNBR remains reduced for 100 µg/mL AgNP (49 %; $p = 0.0079$). Following 48 h exposure to AgNP, MSR is significantly reduced at 30 µg/mL (52 %, $p = 0.0169$). While MSR is decreased at 100 µg/mL AgNP, the effect did not reach significance (54 %, $p = 0.0507$). Similarly, MNBR is decreased by 48 h exposure to AgNP, but without showing a clear dose-effect relation.

3.5. Chronic MEA recordings

Considering the in vivo evidence for long-term accumulation of NP-derived elements in the brain (Lee et al., 2013; Sofranko et al., 2021; Wu et al., 2013; van der Zande et al., 2012), we extended the exposure duration to 14 days and monitored changes in neuronal (network) activity of rat primary cortical cultures following a single exposure to TiO_2NP or AgNP on DIV7.

For TiO_2NP a moderate dose- and time-dependent decrease in neuronal activity is observed (Fig. 6A). MSR is reduced to < 50 % of control at 100 µg/mL TiO_2NP already on DIV17, i.e., 10 days of exposure, while for 30 µg/mL TiO_2NP MSR is reduced to < 50 % of control on DIV21 (14 days of exposure). Effects of TiO_2NP exposure on MNBR are comparable to those on MSR, with > 50 % inhibition observed for 30 µg/mL from DIV17 onwards.

Contrarily, exposure to AgNP clearly reduces neuronal- and network activity of rat primary cortical cultures in a dose- and time-dependent manner, with MNBR being affected earlier and more profound at low doses than MSR (Fig. 6B). AgNP significantly decreases MSR to values < 50 % of control on DIV10 (3 days of exposure) for 100 µg/mL (17 %; $p = < 0.0001$), on DIV14 (7 days of exposure) for 30 µg/mL (3 %; $p = < 0.0001$), on DIV17 (10 days of exposure) for 10 µg/mL (17 %; $p = < 0.0001$), and on DIV21 (14 days of exposure) for 3 µg/mL (3 %; $p = < 0.0001$). Interestingly, from DIV14 (7 days exposure) onwards, MNBR is reduced stronger than MSR, particularly for lower AgNP doses (1–10 µg/mL) e.g. on DIV14 (7 days exposure) MNBR was significantly reduced by 1 µg/mL AgNP (49 %; $p = 0.0218$).

3.6. Cell viability after chronic exposure to TiO2NP and AgNP

To exclude that neurotoxic effects of NP are not simply due to loss of cell viability, metabolic activity of rat primary cortical cells was assessed following chronic exposure to TiO_2NP or AgNP using an Alamar Blue assay. On DIV21, after 14 days chronic exposure, TiO_2NP (1–100 µg/mL) did not adversely affected metabolic activity (Fig. 7A). Our data, however, show that after 14 days exposure to 30 µg/mL and 100 µg/mL AgNP metabolic activity is reduced to 85 % ($p < 0.001$) and 50 % ($p < 0.0001$) of control, respectively, indicative of reduced cell viability.

3.7. Immunohistochemistry

The results of the chronic MEA experiment (Fig. 6) indicate that from DIV10 (3 days of exposure) onwards neuronal (network) activity is strongly reduced, although cell viability (Fig. 7) is affected only at 30 µg/mL and 100 µg/mL AgNP. We, therefore, immunostained neurons and astrocytes in rat primary cortical cultures following 3 days (DIV10), 7 days (DIV14), and 14 days (DIV21) exposure to TiO_2NP (30 µg/mL) and AgNP (3 µg/mL and 30 µg/mL AgNP) to evaluate the morphology of the neuronal network and the supporting astrocyte layer.

Staining of neurons exposed to 30 µg/mL TiO_2NP does not indicate a less confluent neuronal network on DIV21 (14 days exposure; Fig. 8A). Astrocyte staining appears more prominent for TiO_2NP exposed cultures (Fig. 8B), although it should be noted that this observation is likely due to modest autofluorescence of TiO_2NP and unspecific secondary antibody binding to TiO_2NP (see Supplementary data Fig. S4) and not necessarily to increased astrocyte presence in the culture.

Immunohistochemistry of AgNP exposed cells suggests dose- and time-dependent degeneration of the neuronal network and the astrocyte layer (Fig. 8). Neuron staining of cultures exposed to non-cytotoxic AgNP dose (3 µg/mL) only show minor reductions in neuronal network confluency, while MEA recording show a strong disruption of neuronal network activity from DIV14 onwards (Fig. 7B). In contrast, for 30 µg/mL AgNP, the neuronal network exhibits clear holes and morphological changes after 7 days exposure (DIV14; Fig. 8A) potentially explaining the complete cessation of neuronal (network) activity (Fig. 7B). Additionally, staining of S100β shows rounded and enlarged astrocytes on DIV10, which are unusual for rat primary cortical cultures (Fig. 8B, white arrows) and may indicate that astrocytes are affected earlier by high concentration of AgNP than neurons. On DIV21, after 14 days exposure, the astrocyte layer for cultures exposed to 3 µg/mL is starting to show small holes (Fig. 8B, orange arrows), whereas at 30 µg/mL AgNP the astrocyte layer seems to be degrading.

4. Discussion

Our data indicate that exposure to PVP-coated AgNP dose- and time-dependently disrupts spontaneous neuronal (network) activity, ultimately resulting in the complete cessation of neuronal function during chronic exposure. Effects of AgNP on neurophysiological function often

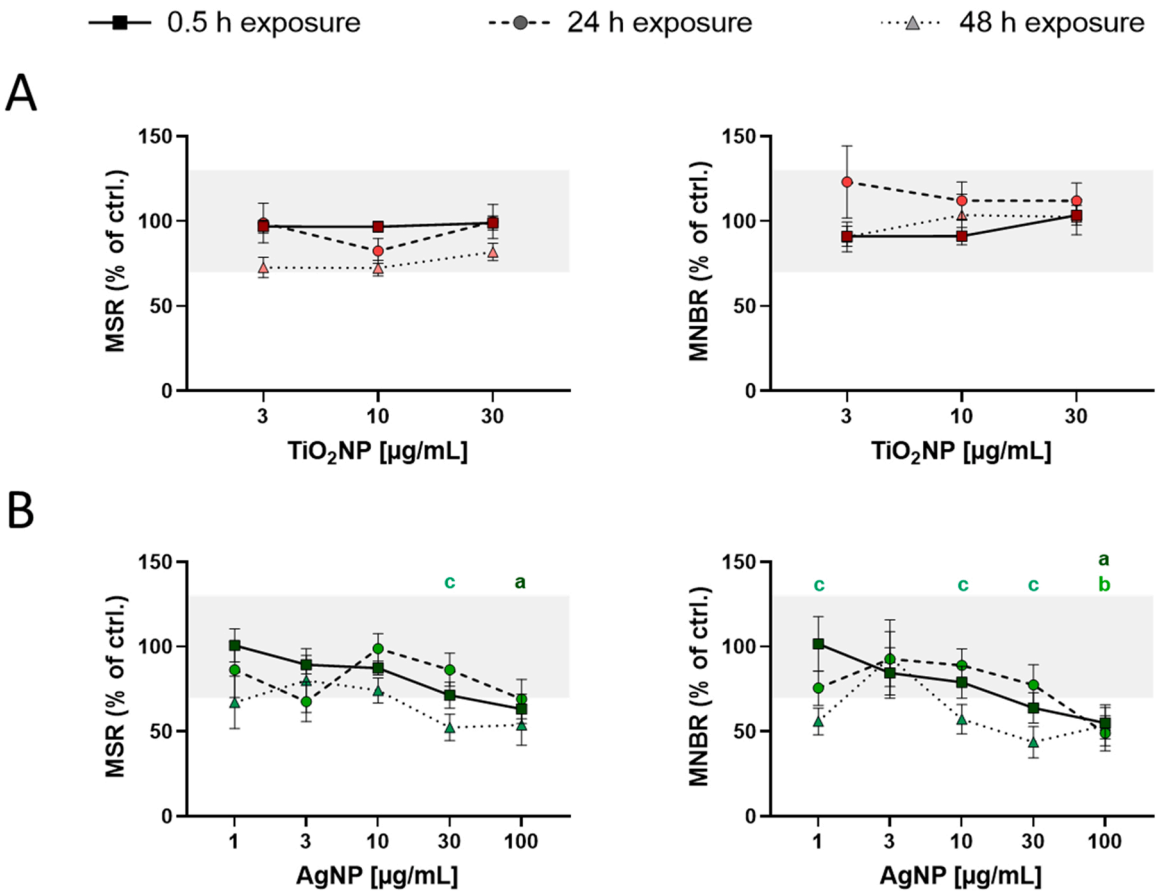

Fig. 5. Acute and sub-chronic effects of TiO_2NP (A) and AgNP (B) on neuronal activity of rat primary cortical cultures. Mean Spike Rate (MSR, left) and Mean Network Burst Rate (MNBR, right) are presented as mean treatment ratio (± SEM) normalized to time-matched controls from n = 9–17 wells from N = 3 plates. Effects ≤ 30 % (i.e. the variation of vehicle control) are considered to be of limited (toxicological) relevance (depicted by the grey area). Relevant effects that are statistically different (Welch's ANOVA) from control are indicated with [a] for 0.5 h exposure ($p < 0.05$), [b] for 24 h exposure ($p < 0.05$), [c] for 48 h exposure ($p < 0.05$).

occur either concomitantly with, or as a result of, cytotoxicity (Skalska et al., 2015). At high AgNP doses (≥ 30 µg/mL), cytotoxicity is indeed likely to impact neuronal activity, but it remains unclear from which DIV cell viability was reduced. Moreover, it is unlikely, that the modest loss of cell viability (85 % compared to control remaining) after 14 days exposure (DIV21; Fig. 7B) to 30 µg/mL AgNP underlies the strong and almost complete inhibition of the neuronal (network) function that is evident already after 7 days exposure (DIV14; Fig. 6B). Further, our immunohistochemical staining of neurons and astrocytes (Fig. 8) shows that from DIV14 onwards (after 7 days of exposure) both cell types were clearly affected by 30 µg/mL AgNP, suggesting that the decrease in neuronal activity (partly) results from morphological changes. Interestingly, after 3 days exposure (on DIV10) to 30 µg/mL AgNP morphological alterations in astrocytes were observed, which may be an indication of astrocytosis, a complex response of astrocytes to injury (Pekny and Pekna, 2014; Sofroniew, 2014). Although we did not quantify the morphological alterations, which hampers further interpretation, morphological changes of astrocytes and their activation were also reported in previous studies in which human embryonic stem cells or rats were exposed to single dose of AgNP for 72 h (Repar et al., 2018) or 24 h (Sharma et al., 2009). In our study, neuronal activity and network function still appeared unaffected when astrocytes already showed morphological changes, suggesting that astrocytes may be more vulnerable to AgNP than neurons. Interestingly, several studies reported that glia cells, including astrocytes and microglia, are more vulnerable to NP exposure than pure neuron cultures (Long et al., 2007a) and that their presence is required to induce adverse effects in neuronal cells (Long et al., 2007b; Xing et al., 2011).

Importantly, on DIV21 (14 days of exposure), exposure to doses below 30 µg/mL AgNP did not affect cell viability or change the morphology of rat primary cortical cultures. Nevertheless, MEA data show a clear reduction in MSR and particularly in MNBR from DIV14 onwards, also at 1 µg/mL and 3 µg/mL. Combined these findings indicate that the decrease in neuronal activity at low doses AgNP is not due to cell death.

In contrast to chronic exposure, acute and sub-chronic AgNP exposure induced only minor changes in spontaneous neuronal activity. Similarly, previous studies using rat primary cortical cells cultured on MEA did not report consistent changes in number of total spikes or active electrodes following acute (1 h), 24 h or 48 h exposure to several sizes and coated AgNP (10–75 nm, PVP- and citrate-coated; Strickland et al., 2016). However, in the same study, cultures exposed for 48 h to 75 nm PVP-coated AgNP and then stimulated with the GABA-receptor antagonist Bicuculline to maximize neuronal activity, did not reach the same activity level as control (Strickland et al., 2016), suggesting that the maximal excitability of the culture was reduced. It is tempting to speculate that this is in line with our results on Ca^{2+} imaging, where 24 h exposure to PVP-coated AgNP reduces net Ca^{2+} influx following K^+-evoked depolarization, thereby likely lowering the overall excitability. However, the inhibition of VGCC is observed only at doses ≥ 10 µg/mL, indicating other targets are involved in the reduction of neuronal activity following chronic exposure. In addition to the inhibition of VGCC, it has also been shown that exposure of rat hippocampal slice preparations to AgNP reduced the voltage-gated sodium current (Liu et al., 2009) and potassium current (Liu et al., 2011) and disrupts glutamatergic neurotransmission (Liu et al., 2012; Ziemińska et al.,

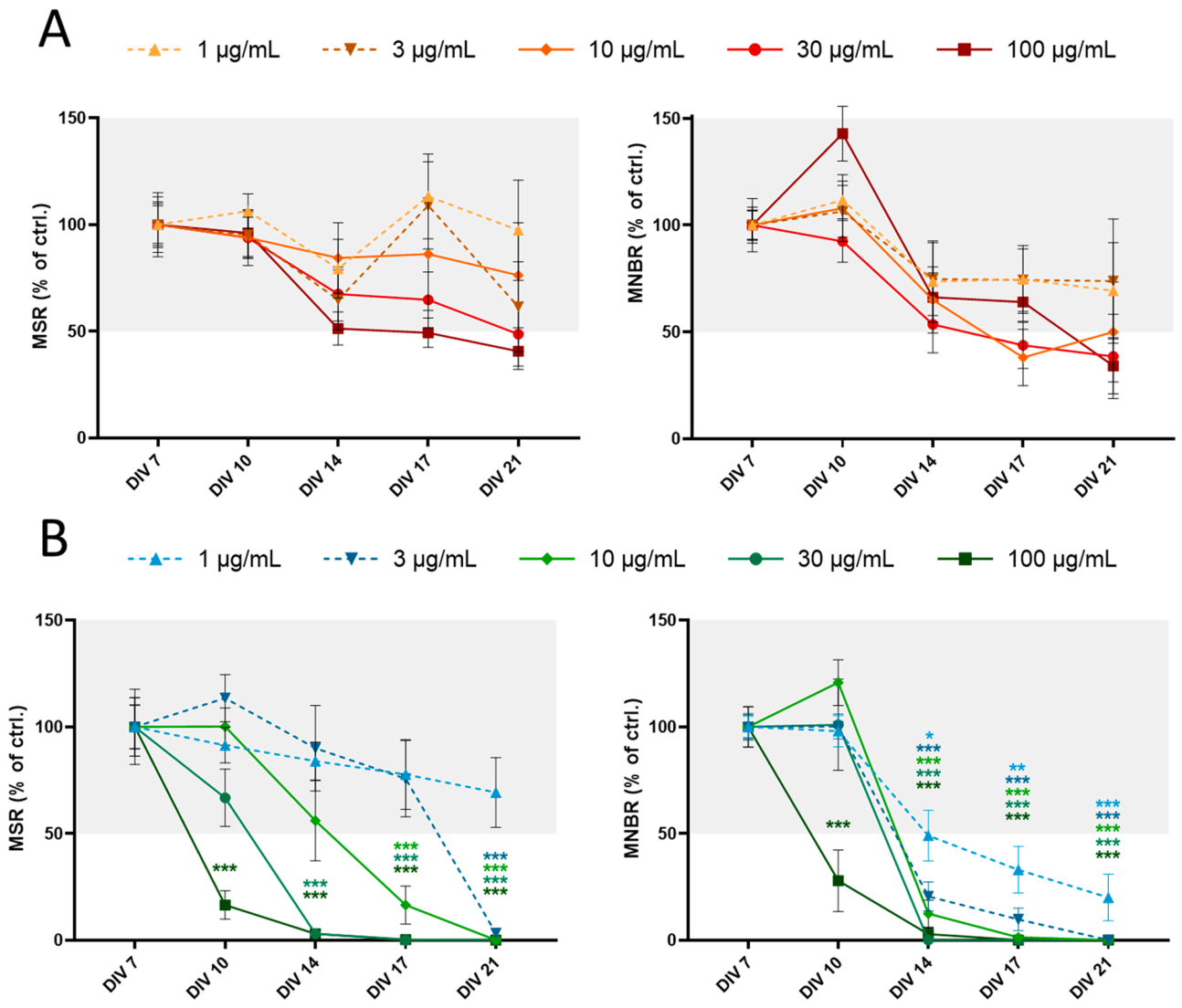

Fig. 6. Chronic effects on neuronal (network) activity following single exposure to TiO_2NP (A) and AgNP (B) in rat primary cortical cultures. Mean Spike Rate (MSR, left) and Mean Network Burst Rate (MNBR, right) are presented as treatment ratio (mean ± SEM) normalized to control from $n = 9$–17 wells from $N = 3$–4 plates. Effects ≤ 50 % (i.e. the variation of vehicle control) are considered to be of limited (toxicological) relevance (depicted by the grey area). Relevant effects that are statistically different (two-way ANOVA) from control are indicated with * ($p < 0.05$), ** ($p < 0.01$), *** ($p < 0.001$).

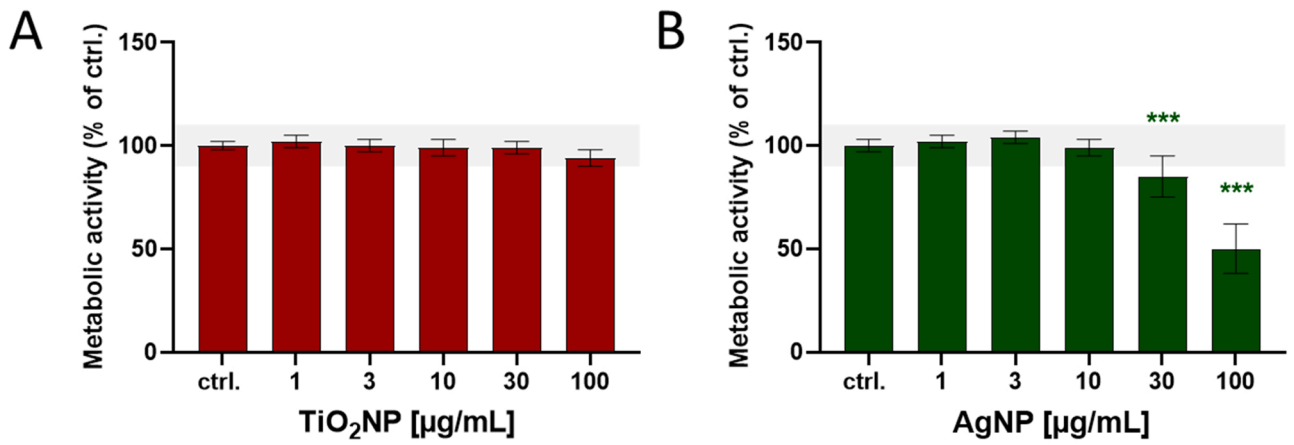

Fig. 7. Metabolic activity of rat primary cortical cells following 14 days exposure to TiO_2NP (A) or AgNP (B). Values are normalized to control and depicted as mean ± SD from n = 21–23 wells from N = 3 plates. Effects ≤ 10 % (i.e. the variation of vehicle control) are considered to be of limited (toxicological) relevance (depicted by the grey area). Relevant effects that are statistically different (one-way ANOVA) from control are indicated with *** ($p < 0.001$).

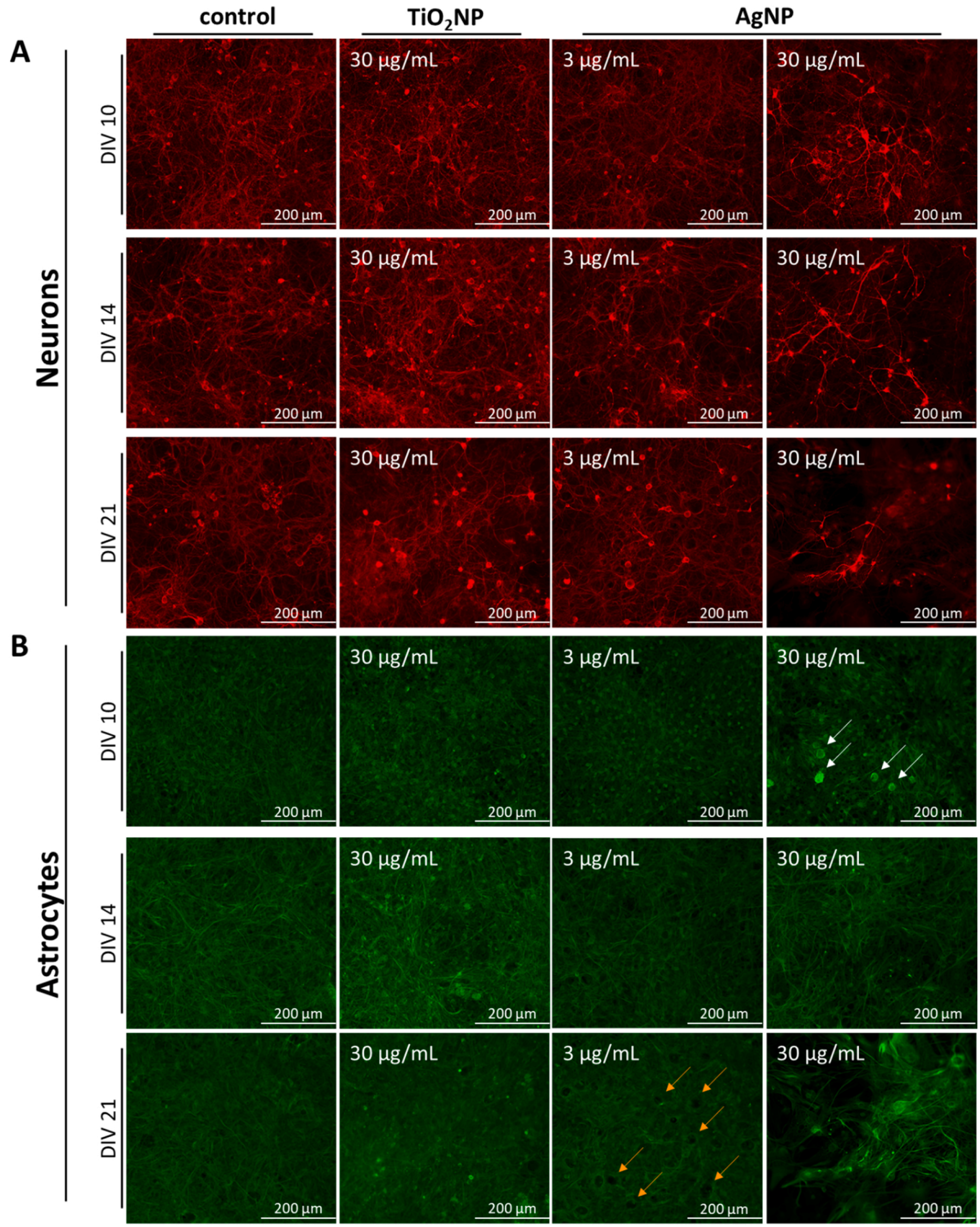

Fig. 8. Morphology of (A) neurons and (B) astrocytes in rat primary cortical cultures after 3 days (DIV10), 7 days (DIV14), and 14 days (DIV21) exposure to TiO_2NP and AgNP. On DIV7, cells were exposed to glutamate-free medium (control), 30 µg/mL TiO_2NP, or 3 and 30 µg/mL AgNP. On DIV10, DIV14, and DIV21 cells were fixed and stained using (A) βIII tubulin (neurons; red) and (B) S100β (astrocytes; green). White arrows indicate morphologically changed astrocytes, whereas orange arrows indicate holes in the astrocyte layer. Images were captured at 200x magnification.

2014), which could all contribute to an overall reduction in excitability.

During the 14 days exposure (DIV7–21), TiO_2NP reduced neuronal activity only modestly (Fig. 6A), without inducing obvious morphological changes (Fig. 8). The decrease in spontaneous neuronal activity occurred only after prolonged exposure and was small compared to the changes induced by AgNP. For these chronic MEA experiments it is, however, important to consider that the spontaneous neuronal activity in controls decreases over time and activity on DIV17 is already very low (Dingemans et al., 2016), which results in high variation in the controls (usually ~50 %) and consequently limiting the sensitivity of the chronic exposure experiments. Nevertheless, the effect following chronic exposure to TiO_2NP should not be discounted as it is dose-dependent and occurred in the absence of cytotoxicity. In contrast, acute and sub-chronic exposure to TiO_2NP clearly did not affect spontaneous neuronal activity (Fig. 5A), depolarization-evoked Ca^{2+} influx (Fig. 4) and viability (Fig. 7). The absence of acute effects on neuronal activity is in apparent contrast to earlier studies that reported a transient reduction in MSR for 25 nm TiO_2NP after 1 h exposure (Strickland et al., 2015). Also, neuronal activity of primary murine cortical networks cultured on MEA was inhibited dose-dependently during 12 h exposure to TiO_2NP (< 100 nm) with effects seen from 1 μg/cm^2 onwards (Gramowski et al., 2010). In our study, the estimated delivered dose after acute (0.5 h) exposure was only 0.1 μg, and 1 μg/cm^2 was only exceeded after 24 h exposure (3.2 μg/cm^2, see Table 2), suggesting that (transient) effects may have been detected if higher dose levels were included in our study. Interestingly, chronic exposure to 100 μg/mL TiO_2NP (simulated deposited dose of 36.2 μg/cm^2 on DIV10 (after 3 days exposure)) resulted in 50 % inhibition of neuronal activity after 7 days exposure (DIV14) suggesting a slow mode of action or further deposition of TiO_2NP.

Induction of oxidative stress, inflammation, and the release of toxic ions are widely considered as the three main molecular mechanisms of action underlying the neurotoxicity of NP (for review see Boyes and van Thriel, 2020). The release of toxic ions as a mode of action is controversially and mainly relevant for relatively soluble metal-based NP, like AgNP, but less for NP that are stable in biological fluids like TiO_2NP (Boyes and van Thriel, 2020; Hadrup and Lam, 2014). Even though AgNP are considered more soluble than TiO_2NP, solubility of AgNP is size-dependent and increases with decreasing size. Under physiological conditions (pH 7), dissolution of AgNP in the size range used in the current study (13 nm and 70 nm) has been demonstrated to be very low (0–2.3 %; Peretyazhko et al., 2014). While the release of toxic ions may (partly) explain the cytotoxic effects observed at high doses AgNP, this could be due to uptake of NPs and lysosomal degradation (Miyayama and Matsuoka, 2016) rather than to extracellular dissolution. This is among others illustrated by the differential neurophysiological changes in primary cortical cells exposed to AgNP vs $AgNO_3$ (Strickland et al., 2016), a silver salt commonly used to expose to ionic Ag (Faunce and Watal, 2010). Similarly, in murine primary cortical networks, the dose-dependent inhibition of the spontaneous neuronal activity induced by TiO_2NP was not in line with the measured ROS levels suggesting that the changes in neuronal activity are unlikely the direct result of oxidative stress (Gramowski et al., 2010). Moreover, AgNP and TiO_2NP change neuronal function also at non-cytotoxic dose levels. Therefore, NP toxicity cannot be explained only by induction of oxidative stress (Gramowski et al., 2010; Strickland et al., 2015) and/or the release of ionic Ag (Garcia-Reyero et al., 2014; Powers et al., 2011; Strickland et al., 2016; Sun et al., 2016). It has been suggested earlier that NP have an additional nanosized-related mode of action (for review see Boyes and van Thriel, 2020), which possibly involves the direct interaction with ion channels and/or neurotransmitter receptors as discussed above.

Physical and chemical characteristics of NP including their size, specific surface area, and coating are crucial for their toxicity (see Sukhanova et al., 2018). NP toxicity is further affected by their behavior and potential agglomeration in biological fluid, with smaller NP being more toxic compared to bigger agglomerates (Christian et al., 2008; Osborne et al., 2013). Additionally, the estimated delivered dose of NP not only highly depends on nanomaterial and agglomerate characteristics but also on the in vitro experimental conditions such as the exposure duration and height of the medium. Combined, these different factors at least partly explain the inconsistency in the reported effects and no observed effect levels for TiO_2NP and AgNP (Skalska and Struzyńska, 2015; Strickland et al., 2016, 2015).

Interestingly, sedimentation simulation by IDSS suggested that the deposition rate of TiO_2NP in the culture medium was ~4 times higher than the rate estimated for AgNP. Thus, even though the applied dose was similar for both NP, the delivered dose for TiO_2NP was much higher compared to the fraction of AgNP depositing on the cells and therefore, our data support that TiO_2NP is clearly less harmful than AgNP. However, scanning electron microscopy and DLS analysis indicate that TiO_2NP and AgNP suspensions contained a large fraction of bulky adducts (>1000 nm; Fig. 2), which likely deposited within 24 h. Therefore, we expect that cells were mainly exposed to agglomerates that have in relation a smaller surface area than primary NP, leading to less reactivity and toxicity (see Foroozandeh and Aziz, 2018) and the toxicity of TiO_2NP and AgNP may be higher in the absence of agglomeration.

When comparing the dose of NP from our in vitro study to animal studies, our lowest applied NP doses are ~20–50 times higher than highest Ti and Ag brain levels reported in exposed animals. Recent in vivo studies exposing rodents for 4–8 weeks to TiO_2NP or AgNP, reported brain levels of 0.004–5.3 μg Ti/g wet tissue (Grissa et al., 2020) and 1–2 Ag μg/g wet tissue (Sofranko et al., 2021). Further, several in vivo findings indicated a rapid and persistent Ag accumulation in the brain supporting concern for chronic exposure effects of AgNP (Lee et al., 2013; van der Zande et al., 2012; Sofranko et al., 2021). Usually, delivered NP doses are considered to be more relevant but since AgNP are soluble and toxicity can be mediated by Ag ions, we decided to compare the applied doses with in vivo brain levels. Assuming that 1 g of tissue equals 1 mL medium, the in vivo Ag brain level of 1–2 μg/g wet tissue (Sofranko et al., 2021) translate to 1–2 μg/mL, which is comparable to the lowest applied in vitro dose of 1 μg/mL in our study suggesting that chronic MEA exposure experiments can be a sensitive alternative for in vivo studies to detect neurotoxic potency of NP.

In conclusion, our findings indicate that TiO_2NP exposure is of limited hazard for neuronal function. In contrast, short term exposure to AgNP inhibits depolarization-evoked calcium influx, whereas chronic AgNP exposure potently disrupts neuronal (network) activity in vitro already at levels comparable to the in vivo brain Ag concentration, therefore causing concern for brain health.

CRediT authorship contribution statement

Lora-Sophie Gerber: Conceptualization, Formal analysis, Writing – original draft, Writing – review & editing. **Harm J. Heusinkveld:** Conceptualization, Formal analysis, Investigation, Supervision, Writing – original draft, Project administration. **Celine Langendoen:** Formal analysis, Investigation. **Burkhard Stahlmecke:** Conceptualization, Methodology, Validation, Investigation, Resources. **Roel PF Schins:** Conceptualization, Methodology, Validation, Writing – review & editing. **Remco HS Westerink:** Conceptualization, Writing – original draft, Writing – review & editing, Supervision, Project administration, Funding acquisition.

Declaration of Competing Interest

The authors declare that they have no known competing financial interests or personal relationships that could have appeared to influence the work reported in this paper.

Acknowledgements

We gratefully acknowledge the members of the Neurotoxicology Research Group for helpful discussions. We thank Bryan Hellack (IUTA e.V. Duisburg, Germany; to date being at the German Environment Agency) for performing the DLS analysis of the NP, and Esther van 't Veld and Richard Wubbolts (Center for Cell Imaging, Utrecht University) for help with the microscopy work. This work was funded by the Dutch-German (ZonMW-BMBF) co-funded project N3RvousSystem (Grant #114027001 ZonMW; FKZ 031L0020A/B BMBF), the European Union's Horizon 2020 Research and Innovation Programme under grant agreement No 814978 (TUBE), and by the Faculty of Veterinary Medicine (Utrecht University, The Netherlands). The authors declare they have no competing financial interests.

Appendix A. Supporting information

Supplementary data associated with this article can be found in the online version at doi:10.1016/j.neuro.2022.10.010.

References

Barclay, J.W., Morgan, A., Burgoyne, R.D., 2005. Calcium-dependent regulation of exocytosis. Cell Calcium 38, 343–353. https://doi.org/10.1016/J.CECA.2005.06.012.

Bencsik, A., Lestaevel, P., Guseva Canu, I., 2018. Nano- and neurotoxicology: an emerging discipline. Prog. Neurobiol. https://doi.org/10.1016/j.pneurobio.2017.10.003.

Bopp, S.K., Lettieri, T., 2008. Comparison of four different colorimetric and fluorometric cytotoxicity assays in a zebrafish liver cell line. BMC Pharm. 8, 8. https://doi.org/10.1186/1471-2210-8-8.

Boyes, W.K., van Thriel, C., 2020. Neurotoxicology of nanomaterials. Chem. Res. Toxicol. https://doi.org/10.1021/acs.chemrestox.0c00050.

Charlesworth, P., Cotterill, E., Morton, A., Grant, S.G.N., Eglen, S.J., 2015. Quantitative differences in developmental profiles of spontaneous activity in cortical and hippocampal cultures. Neural Dev. 10. https://doi.org/10.1186/s13064-014-0028-0.

Christian, P., Von Der Kammer, F., Baalousha, M., Hofmann, T., 2008. Nanoparticles: structure, properties, preparation and behaviour in environmental media. Ecotoxicology. https://doi.org/10.1007/s10646-008-0213-1.

Cohen, J.M., Teeguarden, J.G., Demokritou, P., 2014. An integrated approach for the in vitro dosimetry of engineered nanomaterials. Part. Fibre Toxicol. 11, 1–12. https://doi.org/10.1186/1743-8977-11-20.

DeLoid, G., Cohen, J.M., Darrah, T., Derk, R., Rojanasakul, L., Pyrgiotakis, G., Wohlleben, W., Demokritou, P., 2014. Estimating the effective density of engineered nanomaterials for in vitro dosimetry. Nat. Commun. 5. https://doi.org/10.1038/ncomms4514.

Dingemans, M.M.L., Schütte, M.G., Wiersma, D.M.M., de Groot, A., van Kleef, R.G.D.M., Wijnolts, F.M.J., Westerink, R.H.S., 2016. Chronic 14-day exposure to insecticides or methylmercury modulates neuronal activity in primary rat cortical cultures. Neurotoxicology 57, 194–202. https://doi.org/10.1016/j.neuro.2016.10.002.

Faunce, T., Watal, A., 2010. Nanosilver and global public health: international regulatory issues. https://doi.org/10.2217/nnm.10.33 5, 617–632. https://doi.org/10.2217/NNM.10.33.

Foroozandeh, P., Aziz, A.A., 2018. Insight into cellular uptake and intracellular trafficking of nanoparticles. Nanoscale Res. Lett. 2018 (131 13), 1–12. https://doi.org/10.1186/S11671-018-2728-6.

Gao, X., Yin, S., Tang, M., Chen, J., Yang, Z., Zhang, W., Chen, L., Yang, B., Li, Z., Zha, Y., Ruan, D., Wang, M., 2011. Effects of developmental exposure to TiO2 nanoparticles on synaptic plasticity in hippocampal dentate gyrus area: an in vivo study in anesthetized rats. Biol. Trace Elem. Res. 143, 1616–1628. https://doi.org/10.1007/S12011-011-8990-4.

Garcia-Reyero, N., Kennedy, A.J., Escalon, B.L., Habib, T., Laird, J.G., Rawat, A., Wiseman, S., Hecker, M., Denslow, N., Steevens, J.A., Perkins, E.J., 2014. Differential effects and potential adverse outcomes of ionic silver and silver nanoparticles in vivo and in vitro. Environ. Sci. Technol. 48, 4546–4555. https://doi.org/10.1021/ES4042258/SUPPL_FILE/ES4042258_SI_002.XLSX.

Geraets, L., Oomen, A.G., Krystek, P., Jacobsen, N.R., Wallin, H., Laurentie, M., Verharen, H.W., Brandon, E.F.A., de Jong, W.H., 2014. Tissue distribution and elimination after oral and intravenous administration of different titanium dioxide nanoparticles in rats. Part. Fibre Toxicol. 11, 1–21. https://doi.org/10.1186/1743-8977-11-30.

Gerber, L.-S., Melis, L.V.J., van, Kleef, R.G.D.M., van, Groot, A., de, Westerink, R.H.S., 2021. Culture of rat primary cortical cells for microelectrode array (Mea) recordings to screen for acute and developmental neurotoxicity. Curr. Protoc. 1, e158 https://doi.org/10.1002/CPZ1.158.

Gramowski, A., Flossdorf, J., Bhattacharya, K., Jonas, L., Lantow, M., Rahman, Q., Schiffmann, D., Weiss, D.G., Dopp, E., 2010. Nanoparticles induce changes of the electrical activity of neuronal networks on microelectrode array neurochips. Environ. Health Perspect. 118, 1363–1369. https://doi.org/10.1289/ehp.0901661.

Grissa, I., ElGhoul, J., Mrimi, R., Mir, L., El, Cheikh, H., Ben, Horcajada, P., 2020. In deep evaluation of the neurotoxicity of orally administered TiO2 nanoparticles. Brain Res. Bull. 155, 119–128. https://doi.org/10.1016/J.BRAINRESBULL.2019.10.005.

Guo, Z., Zhang, P., Luo, Y., Xie, H.Q., Chakraborty, S., Monikh, F.A., Bu, L., Liu, Y., Ma, Y., Zhang, Z., Valsami-Jones, E., Zhao, B., Lynch, I., 2020. Intranasal exposure to ZnO nanoparticles induces alterations in cholinergic neurotransmission in rat brain. Nano Today 35, 100977. https://doi.org/10.1016/j.nantod.2020.100977.

Hadrup, N., Lam, H.R., 2014. Oral toxicity of silver ions, silver nanoparticles and colloidal silver – a review. Regul. Toxicol. Pharmacol. 68, 1–7. https://doi.org/10.1016/J.YRTPH.2013.11.002.

Heusinkveld, H.J., van Vliet, A.C., Nijssen, P.C.G., Westerink, R.H.S., 2016. In vitro neurotoxic hazard characterisation of dinitrophenolic herbicides. Toxicol. Lett. 252, 62–69. https://doi.org/10.1016/J.TOXLET.2016.04.014.

Hinderliter, P.M., Minard, K.R., Orr, G., Chrisler, W.B., Thrall, B.D., Pounds, J.G., Teeguarden, J.G., 2010. ISDD: a computational model of particle sedimentation, diffusion and target cell dosimetry for in vitro toxicity studies. Part. Fibre Toxicol. 7, 1–20. https://doi.org/10.1186/1743-8977-7-36.

Hondebrink, L., Verboven, A.H.A., Drega, W.S., Schmeink, S., de Groot, M.W.G.D.M., van Kleef, R.G.D.M., Wijnolts, F.M.J., de Groot, A., Meulenbelt, J., Westerink, R.H.S., 2016. Neurotoxicity screening of (illicit) drugs using novel methods for analysis of microelectrode array (MEA) recordings. Neurotoxicology 55, 1–9. https://doi.org/10.1016/j.neuro.2016.04.020.

Hu, R., Gong, X., Duan, Y., Li, N., Che, Y., Cui, Y., Zhou, M., Liu, C., Wang, H., Hong, F., 2010. Neurotoxicological effects and the impairment of spatial recognition memory in mice caused by exposure to TiO2 nanoparticles. Biomaterials 31, 8043–8050. https://doi.org/10.1016/j.biomaterials.2010.07.011.

Hu, R., Zheng, L., Zhang, T., Gao, G., Cui, Y., Cheng, Z., Cheng, J., Hong, M., Tang, M., Hong, F., 2011. Molecular mechanism of hippocampal apoptosis of mice following exposure to titanium dioxide nanoparticles. J. Hazard. Mater. 191, 32–40. https://doi.org/10.1016/J.JHAZMAT.2011.04.027.

Inshakova, E., Inshakov, O., 2017. World market for nanomaterials: Structure and trends, in: MATEC Web of Conferences. https://doi.org/10.1051/matecconf/201712902013.

Kämpfer, A.A.M., Busch, M., Büttner, V., Bredeck, G., Stahlmecke, B., Hellack, B., Masson, I., Sofranko, A., Albrecht, C., Schins, R.P.F., 2021. Model complexity as determining factor for in vitro nanosafety studies: effects of silver and titanium dioxide nanomaterials in intestinal models. Small 17, 2004223. https://doi.org/10.1002/SMLL.202004223.

Kreyling, W.G., Holzwarth, U., Schleh, C., Kozempel, J., Wenk, A., Haberl, N., Hirn, S., Schäffler, M., Lipka, J., Semmler-Behnke, M., Gibson, N., 2017. Quantitative biokinetics of titanium dioxide nanoparticles after oral application in rats: Part 2. Nanotoxicology 11, 443–453. https://doi.org/10.1080/17435390.2017.1306893.

Lee, J.H., Kim, Y.S., Song, K.S., Ryu, H.R., Sung, J.H., Park, J.D., Park, H.M., Song, N.W., Shin, B.S., Marshak, D., Ahn, K., Lee, J.E., Yu, I.J., 2013. Biopersistence of silver nanoparticles in tissues from Sprague-Dawley rats. Part. Fibre Toxicol. 10. https://doi.org/10.1186/1743-8977-10-36.

Li, Y., Li, J., Yin, J., Li, W., Kang, C., Huang, Q., Li, Q., 2010. Systematic influence induced by 3 nm titanium dioxide following intratracheal instillation of mice. J. Nanosci. Nanotechnol. J. Nanosci. Nanotechnol. 8544–8549. https://doi.org/10.1166/jnn.2010.2690.

Liu, Z., Ren, G., Zhang, T., Yang, Z., 2009. Action potential changes associated with the inhibitory effects on voltage-gated sodium current of hippocampal CA1 neurons by silver nanoparticles. Toxicology 264, 179–184. https://doi.org/10.1016/j.tox.2009.08.005.

Liu, Z., Ren, G., Zhang, T., Yang, Z., 2011. The inhibitory effects of nano-Ag on voltage-gated potassium currents of hippocampal CA1 neurons. Environ. Toxicol. 26, 552–558. https://doi.org/10.1002/tox.20586.

Liu, Z., Zhang, T., Ren, G., Yang, Z., 2012. Nano-Ag inhibiting action potential independent glutamatergic synaptic transmission but increasing excitability in rat CA1 pyramidal neurons. Nanotoxicology 6, 414–423. https://doi.org/10.3109/17435390.2011.583996.

Long, T.C., Tajuba, J., Sama, P., Saleh, N., Swartz, C., Parker, J., Hester, S., Lowry, G.V., Veronesi, B., 2007a. Nanosize titanium dioxide stimulates reactive oxygen species in brain microglia and damages neurons in vitro. Environ. Health Perspect. 115, 1631–1637. https://doi.org/10.1289/ehp.10216.

Long, T.C., Tajuba, J., Sama, P., Saleh, N., Swartz, C., Parker, J., Hester, S., Lowry, G.V., Veronesi, B., 2007b. Nanosize titanium dioxide stimulates reactive oxygen species in brain microglia and damages neurons in vitro. Environ. Health Perspect. 115, 1631–1637. https://doi.org/10.1289/EHP.10216.

Mattson, M.R., 2007. Calcium and neurodegeneration. Aging Cell. https://doi.org/10.1111/j.1474-9726.2007.00275.x.

Miyayama, T., Matsuoka, M., 2016. Involvement of lysosomal dysfunction in silver nanoparticle-induced cellular damage in A549 human lung alveolar epithelial cells. J. Occup. Med. Toxicol. 11, 1–6. https://doi.org/10.1186/S12995-016-0090-0/FIGURES/6.

Nicolas, J., Hendriksen, P.J.M., van Kleef, R.G.D.M., de Groot, A., Bovee, T.F.H., Rietjens, I.M.C.M., Westerink, R.H.S., 2014. Detection of marine neurotoxins in food safety testing using a multielectrode array. Mol. Nutr. Food Res. 58, 2369–2378. https://doi.org/10.1002/mnfr.201400479.

Oberdörster, G., Sharp, Z., Atudorei, V., Elder, A., Gelein, R., Kreyling, W., Cox, C., 2004. Translocation of inhaled ultrafine particles to the brain. Inhal. Toxicol. Inhal. Toxicol. 437–445. https://doi.org/10.1080/08958370490439597.

Oberdörster, G., Oberdörster, E., Oberdörster, J., 2005. Nanotoxicology: an emerging discipline evolving from studies of ultrafine particles. Environ. Health Perspect. https://doi.org/10.1289/ehp.7339.
Oberdörster, G., Elder, A., Rinderknecht, A., 2009. Nanoparticles and the brain: cause for concern? J. Nanosci. Nanotechnol. 9, 4996.
Osborne, O.J., Johnston, B.D., Moger, J., Balousha, M., Lead, J.R., Kudoh, T., Tyler, C.R., 2013. Effects of particle size and coating on nanoscale Ag and TiO2 exposure in zebrafish (Danio rerio) embryos. Nanotoxicology 7, 1315–1324. https://doi.org/10.3109/17435390.2012.737484/SUPPL_FILE/INAN_A_737484_SM0001.DOC.
Pekny, M., Pekna, M., 2014. Astrocyte reactivity and reactive astrogliosis: costs and benefits. Physiol. Rev. 94, 1077–1098. https://doi.org/10.1152/PHYSREV.00041.2013.
Peretyazhko, T.S., Zhang, Q., Colvin, V.L., 2014. Size-controlled dissolution of silver nanoparticles at neutral and acidic pH conditions: kinetics and size changes. Environ. Sci. Technol. 48, 11954–11961. https://doi.org/10.1021/ES5023202/SUPPL_FILE/ES5023202_SI_001.PDF.
Powers, C.M., Badireddy, A.R., Ryde, I.T., Seidler, F.J., Slotkin, T.A., 2011. Silver nanoparticles compromise neurodevelopment in PC12 cells: critical contributions of silver ion, particle size, coating, and composition. Environ. Health Perspect. 119, 37. https://doi.org/10.1289/EHP.1002337.
Repar, N., Li, H., Aguilar, J.S., Li, Q.Q., Drobne, D., Hong, Y., 2018. Silver nanoparticles induce neurotoxicity in a human embryonic stem cell-derived neuron and astrocyte network. Nanotoxicology 12, 104–116. https://doi.org/10.1080/17435390.2018.1425497.
Sharma, H.S., Sharma, A., 2012. Neurotoxicity of engineered nanoparticles from metals. CNS Neurol. Disord. - Drug Targets 11, 65–80. https://doi.org/10.2174/187152712799960817.
Sharma, H.S., Hussain, S., Schlager, J., Ali, S.F., Sharma, A., 2009. Influence of nanoparticles on blood-brain barrier permeability and brain edema formation in rats. In: Acta Neurochirurgica, Supplementum. Springer-Verlag, Wien, pp. 359–364. https://doi.org/10.1007/978-3-211-98811-4_65.
Shi, H., Magaye, R., Castranova, V., Zhao, J., 2013. Titanium dioxide nanoparticles: a review of current toxicological data. Part. Fibre Toxicol. https://doi.org/10.1186/1743-8977-10-15.
Shukla, R.K., Sharma, V., Pandey, A.K., Singh, S., Sultana, S., Dhawan, A., 2011. ROS-mediated genotoxicity induced by titanium dioxide nanoparticles in human epidermal cells. Toxicol. Vitr 25, 231–241. https://doi.org/10.1016/j.tiv.2010.11.008.
Skalska, J., Struzyńska, L., 2015. Toxic effects of silver nanoparticles in mammals–does a risk of neurotoxicity exist? Folia Neuropathol. 53, 281–300. https://doi.org/10.5114/FN.2015.56543.
Skalska, J., Frontczak-Baniewicz, M., Struzyńska, L., 2015. Synaptic degeneration in rat brain after prolonged oral exposure to silver nanoparticles. Neurotoxicology 46, 145–154. https://doi.org/10.1016/j.neuro.2014.11.002.
Skalska, J., Dąbrowska-Bouta, B., Strużyńska, L., 2016. Oxidative stress in rat brain but not in liver following oral administration of a low dose of nanoparticulate silver. Food Chem. Toxicol. 97, 307–315. https://doi.org/10.1016/j.fct.2016.09.026.
Sofranko, A., Wahle, T., Heusinkveld, H.J., Stahlmecke, B., Dronov, M., Pijnenburg, D., Hilhorst, R., Lamann, K., Albrecht, C., Schins, R.P.F., 2021. Evaluation of the neurotoxic effects of engineered nanomaterials in C57BL/6J mice in 28-day oral exposure studies. Neurotoxicology 84, 155–171. https://doi.org/10.1016/J.NEURO.2021.03.005.
Sofroniew, M.V., 2014. Astrogliosis. Cold Spring Harb. Perspect. Biol. 7. https://doi.org/10.1101/CSHPERSPECT.A020420.
Strickland, J.D., LeFew, W.R., Crooks, J., Hall, D., Ortenzio, J.N., Dreher, K., Shafer, T.J., 2015. In vitro screening of metal oxide nanoparticles for effects on neural function using cortical networks on microelectrode arrays. Nanotoxicology 10, 619–628. https://doi.org/10.3109/17435390.2015.1107142.
Strickland, J.D., LeFew, W.R., Crooks, J., Hall, D., Ortenzio, J.N.R., Dreher, K., Shafer, T.J., 2016. In vitro screening of silver nanoparticles and ionic silver using neural networks yields differential effects on spontaneous activity and pharmacological responses. Toxicology 355–356, 1–8. https://doi.org/10.1016/j.tox.2016.05.009.
Strużyńska, L., Skalska, J., 2018. Mechanisms underlying neurotoxicity of silver nanoparticles. In: Advances in Experimental Medicine and Biology. Springer, New York LLC, pp. 227–250. https://doi.org/10.1007/978-3-319-72041-8_14.
Sukhanova, A., Bozrova, S., Sokolov, P., Berestovoy, M., Karaulov, A., Nabiev, I., 2018. Dependence of nanoparticle toxicity on their physical and chemical properties. Nanoscale Res. Lett. 13. https://doi.org/10.1186/S11671-018-2457-X.
Sun, C., Yin, N., Wen, R., Liu, W., Jia, Y., Hu, L., Zhou, Q., Jiang, G., 2016. Silver nanoparticles induced neurotoxicity through oxidative stress in rat cerebral astrocytes is distinct from the effects of silver ions. Neurotoxicology 52, 210–221. https://doi.org/10.1016/J.NEURO.2015.09.007.
Tang, J., Xiong, L., Wang, S., Wang, J., Liu, L., Li, J., Yuan, F., Xi, T., 2009. Distribution, translocation and accumulation of silver nanoparticles in rats. J. Nanosci. Nanotechnol. 9, 4924–4932. https://doi.org/10.1166/jnn.2009.1269.
Tang, J., Xiong, L., Zhou, G., Wang, S., Wang, J., Liu, L., Li, J., Yuan, F., Lu, S., Wan, Z., Chou, L., Xi, T., 2010. Silver nanoparticles crossing through and distribution in the blood-brain barrier in vitro. J. Nanosci. Nanotechnol. 10, 6313–6317. https://doi.org/10.1166/jnn.2010.2625.
Teleanu, D.M., Chircov, C., Grumezescu, A.M., Volceanov, A., Teleanu, R.I., 2018. Impact of nanoparticles on brain health: an up to date overview. J. Clin. Med. 7, 490. https://doi.org/10.3390/JCM7120490.
Teleanu, D.M., Chircov, C., Grumezescu, A.M., Teleanu, R.I., 2019. Neurotoxicity of nanomaterials: an up-to-date overview. Nanomaterials. https://doi.org/10.3390/nano9010096.
Trouiller, B., Reliene, R., Westbrook, A., Solaimani, P., Schiestl, R.H., 2009. Titanium dioxide nanoparticles induce DNA damage and genetic instability in vivo in mice. Cancer Res. 69, 8784–8789. https://doi.org/10.1158/0008-5472.CAN-09-2496.
Tukker, A.M., De Groot, M.W.G.D.M., Wijnolts, F.M.J., Kasteel, E.E.J., Hondebrink, L., Westerink, R.H.S., 2016. Research article is the time right for in vitro neurotoxicity testing using human iPSC-derived neurons? ALTEX 33, 261–271. https://doi.org/10.14573/altex.1510091.
Van Der Zande, M., Vandebriel, R.J., Van Doren, E., Kramer, E., Herrera Rivera, Z., Serrano-Rojero, C.S., Gremmer, E.R., Mast, J., Peters, R.J.B., Hollman, P.C.H., Hendriksen, P.J.M., Marvin, H.J.P., Peijnenburg, A.A.C.M., Bouwmeester, H., 2012. Distribution, elimination, and toxicity of silver nanoparticles and silver ions in rats after 28-day oral exposure. ACS Nano 6, 7427–7442. https://doi.org/10.1021/NN302649P.
Wang, J., Chen, C., Liu, Y., Jiao, F., Li, W., Lao, F., Li, Y., Li, B., Ge, C., Zhou, G., Gao, Y., Zhao, Y., Chai, Z., 2008a. Potential neurological lesion after nasal instillation of TiO2 nanoparticles in the anatase and rutile crystal phases. Toxicol. Lett. 183, 72–80. https://doi.org/10.1016/j.toxlet.2008.10.001.
Wang, J., Liu, Y., Jiao, F., Lao, F., Li, W., Gu, Y., Li, Y., Ge, C., Zhou, G., Li, B., Zhao, Y., Chai, Z., Chen, C., 2008b. Time-dependent translocation and potential impairment on central nervous system by intranasally instilled TiO2 nanoparticles. Toxicology 254, 82–90. https://doi.org/10.1016/j.tox.2008.09.014.
Weir, A., Westerhoff, P., Fabricius, L., Hristovski, K., Von Goetz, N., 2012. Titanium dioxide nanoparticles in food and personal care products. Environ. Sci. Technol. 46, 2242–2250. https://doi.org/10.1021/es204168d.
Westerink, R., 2006. Targeting exocytosis: Ins and outs of the modulation of quantal dopamine release. CNS Neurol. Disord. - Drug Targets 5, 57–77. https://doi.org/10.2174/187152706784111597.
Wu, J., Ding, T., Sun, J., 2013. Neurotoxic potential of iron oxide nanoparticles in the rat brain striatum and hippocampus. Neurotoxicology 34, 243–253. https://doi.org/10.1016/J.NEURO.2012.09.006.
Xing, B., Bachstetter, A.D., Van Eldik, L.J., 2011. Microglial p38a MAPK is critical for LPS-induced neuron degeneration, through a mechanism involving TNFa. https://doi.org/10.1186/1750–1326-6–84.
Xu, F., Piett, C., Farkas, S., Qazzaz, M., Syed, N.I., 2013. Silver nanoparticles (AgNPs) cause degeneration of cytoskeleton and disrupt synaptic machinery of cultured cortical neurons. Mol. Brain 6, 1–15. https://doi.org/10.1186/1756-6606-6-29.
Yokel, R., Grulke, E., MacPhail, R., 2013. Metal-based nanoparticle interactions with the nervous system: the challenge of brain entry and the risk of retention in the organism. Wiley Interdiscip. Rev. Nanomed. Nanobiotechnology 5, 346–373. https://doi.org/10.1002/wnan.1202.
Yokel, R.A., Macphail, R.C., 2011. Engineered nanomaterials: exposures, hazards, and risk prevention, Journal of Occupational Medicine and Toxicology 2011 6:1. BioMed Central. https://doi.org/10.1186/1745–6673-6–7.
Ze, Y., Hu, R., Wang, X., Sang, X., Ze, X., Li, B., Su, J., Wang, Y., Guan, N., Zhao, X., Gui, S., Zhu, L., Cheng, Z., Cheng, J., Sheng, L., Sun, Q., Wang, L., Hong, F., 2014. Neurotoxicity and gene-expressed profile in brain-injured mice caused by exposure to titanium dioxide nanoparticles. J. Biomed. Mater. Res. Part A 102, 470–478. https://doi.org/10.1002/JBM.A.34705.
Ziemińska, E., Stafiej, A., Struzyńska, L., 2014. The role of the glutamatergic NMDA receptor in nanosilver-evoked neurotoxicity in primary cultures of cerebellar granule cells. Toxicology 315, 38–48. https://doi.org/10.1016/j.tox.2013.11.008.